



# Evolutionary Phases of Gas-rich Galaxies in a Galaxy Cluster at $z = 1.46$

Masao Hayashi<sup>1</sup>, Tadayuki Kodama<sup>1,2,3</sup>, Kotaro Kohno<sup>4,5</sup>, Yuki Yamaguchi<sup>4</sup>, Ken-ichi Tadaki<sup>1,6</sup>, Bunyo Hatsukade<sup>4</sup>, Yusei Koyama<sup>2,7</sup>, Rhythm Shimakawa<sup>1,8</sup>, Yoichi Tamura<sup>4,9</sup>, and Tomoko L. Suzuki<sup>1</sup>

<sup>1</sup> National Astronomical Observatory of Japan, Osawa, Mitaka, Tokyo 181-8588, Japan; [masao.hayashi@nao.ac.jp](mailto:masao.hayashi@nao.ac.jp)

<sup>2</sup> Department of Astronomical Science, SOKENDAI (The Graduate University for Advanced Studies), Mitaka, Tokyo 181-8588, Japan

<sup>3</sup> Astronomical Institute, Tohoku University, Aramaki, Aoba-ku, Sendai 980-8578, Japan

<sup>4</sup> Institute of Astronomy, The University of Tokyo, Osawa, Mitaka, Tokyo 181-0015, Japan

<sup>5</sup> Research Center for the Early Universe, The University of Tokyo, 7-3-1 Hongo, Bunkyo, Tokyo 113-0033, Japan

<sup>6</sup> Max-Planck-Institut für Extraterrestrische Physik, Giessenbachstrasse, D-85748 Garching, Germany

<sup>7</sup> Subaru Telescope, National Astronomical Observatory of Japan, 650 North A'ohoku Place, Hilo, HI 96720, USA

<sup>8</sup> UCO/Lick Observatory, University of California, 1156 High Street, Santa Cruz, CA 95064, USA

<sup>9</sup> Department of Physics, Nagoya University, Furo-cho, Chikusa-ku, Nagoya 464-8601, Japan

Received 2017 February 17; revised 2017 May 5; accepted 2017 May 6; published 2017 May 24

## Abstract

We report a survey of molecular gas in galaxies in the XMMXCS J2215.9–1738 cluster at  $z = 1.46$ . We have detected emission lines from 17 galaxies within a radius of  $R_{200}$  from the cluster center, in Band 3 data of the Atacama Large Millimeter/submillimeter Array, with a coverage of 93–95 GHz in frequency and 2.33 arcmin<sup>2</sup> in spatial direction. The lines are all identified as CO  $J = 2-1$  emission lines from cluster members at  $z \sim 1.46$  by their redshifts and the colors of their optical and near-infrared (NIR) counterparts. The line luminosities reach down to  $L'_{\text{CO}(2-1)} = 4.5 \times 10^9 \text{ K km s}^{-1} \text{ pc}^2$ . The spatial distribution of galaxies with a detection of CO(2–1) suggests that they disappear from the very center of the cluster. The phase-space diagram showing relative velocity versus cluster-centric distance indicates that the gas-rich galaxies have entered the cluster more recently than the gas-poor star-forming galaxies and passive galaxies located in the virialized region of this cluster. The results imply that the galaxies experienced ram-pressure stripping and/or strangulation during the course of infall toward the cluster center and then the molecular gas in the galaxies at the cluster center was depleted by star formation.

**Key words:** galaxies: clusters: individual (XMMXCS J2215.9–1738) – galaxies: evolution – galaxies: ISM

## 1. Introduction

Identifying the physical mechanisms that cause quenching of star formation in galaxies is one of the critical outstanding issues regarding galaxy formation and evolution. Given that galaxy clusters in the local Universe are dominated by quiescent early-type galaxies (e.g., Dressler et al. 1997; Peng et al. 2010; Scoville et al. 2013), the environment where galaxies reside must play a vital role in quenching their star formation activities, which eventually turns them into passively evolving elliptical or S0 galaxies. Although various processes that could be responsible for the environmental quenching are considered, such as, for example, major/minor mergers, ram-pressure stripping, and strangulation, the central process that governs the star formation activity and quenching in cluster galaxies has yet to be identified.

The gas content of galaxies is a fundamental quantity that is directly related to the star formation activities in galaxies. The gas-regulated models predict that the amount of molecular gas that galaxies contain can govern the scaling relations such as the mass–star formation rate (SFR) main-sequence and mass–metallicity relation (Lilly et al. 2013; Zahid et al. 2014). Indeed, the gas fraction is known to be larger in galaxies at higher redshifts up to  $z \gtrsim 2$ , and the SFR of a galaxy with a given mass also becomes larger in proportion to the gas fraction as the redshift increases (e.g., Tacconi et al. 2010; Geach et al. 2011; Saintonge et al. 2013). Since star-forming galaxies in high- $z$  galaxy clusters should grow to massive early-type galaxies in the local universe, the cluster galaxies' gas contents allow us to better understand the quenching mechanisms of galaxies in dense environments. However, most of the observations of molecular gas at high redshifts have been

limited to the galaxies in general fields (e.g., Carilli & Walter 2013; Walter et al. 2014; Genzel et al. 2015; Silverman et al. 2015; Decarli et al. 2016; Seko et al. 2016; Tacconi et al. 2017). Although several studies have surveyed molecular gas in galaxy (proto-)clusters at  $z \approx 1-3$ , CO emissions are detected from at most a few member galaxies in each cluster (Aravena et al. 2012; Casasola et al. 2013; Ivison et al. 2013; Tadaki et al. 2014; Dannerbauer et al. 2017).

The XMMXCS J2215.9–1738 galaxy cluster at  $z = 1.457$  (22<sup>h</sup>15<sup>m</sup>58<sup>s</sup>.5,  $-17^{\circ}38'02''$ .5; Stanford et al. 2006) is one of the best-studied high- $z$  galaxy clusters. Hayashi et al. (2010, 2014) conducted deep narrowband imaging with Suprime-Cam/Subaru targeting [O II] emission lines from galaxies in this cluster. The observation with Suprime-Cam/Subaru has identified many star-forming galaxies in the core region (see also Hilton et al. 2010; Ma et al. 2015), which suggests that the massive galaxies in the cluster core are still in their formation phase and are as active as those in the general field at similar redshifts. This galaxy cluster is one of the best targets to probe the early phases of environmental quenching processes.

This Letter focuses on Atacama Large Millimeter/submillimeter Array (ALMA) detection of CO  $J = 2-1$  ( $\nu_{\text{rest}} = 230.538 \text{ GHz}$ ) emission lines in the  $z = 1.46$  galaxy cluster and presents global properties of molecular gas contents of the cluster galaxies. More detailed characteristics of the individual galaxies will be discussed in forthcoming papers. The velocity dispersion of the cluster member galaxies is  $\sigma = 720 \text{ km s}^{-1}$  and the radius of the galaxy cluster is  $R_{200} = 0.8 \text{ Mpc}$  (Hilton et al. 2010). The cosmological parameters of  $H_0 = 70 \text{ km s}^{-1} \text{ Mpc}^{-1}$ ,  $\Omega_m = 0.3$ , and  $\Omega_\Lambda = 0.7$  are adopted.

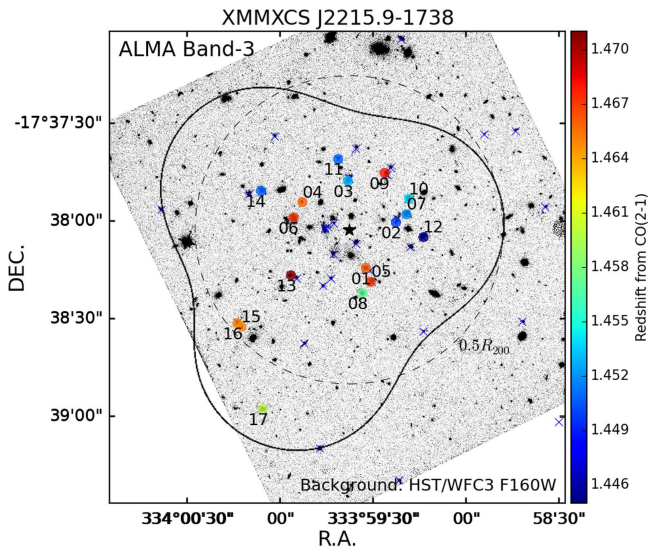


**Figure 1.** Spatial distribution of galaxies, with detections of CO(2–1) lines shown by filled circles. They are color-coded based on the redshifts estimated from the CO(2–1) lines, and the numbers next to the symbols show the IDs of the galaxies (see Table 1). The solid curve shows a region where the ALMA Band 3 data are available with a sensitivity greater than 50%. The cross symbols show the [O II] emitters associated with this cluster (Hayashi et al. 2014). A star symbol shows a cluster center determined with extended X-ray emission (Stanford et al. 2006). The background is the *HST*/WFC3 image in F160W. The dashed circle shows the cluster-centric radius of  $0.5R_{200}$  (Hilton et al. 2010).

## 2. Data

Our ALMA Cycle 3 program in Band 3, 2015.1.00779.S, was conducted in 2016 May. The spectral coverage is 93.03–94.86 GHz with a spectral resolution of 13.906 MHz ( $\sim 12.5 \text{ km s}^{-1}$ ), which allows us to capture CO(2–1) emission lines from galaxies at  $z = 1.430\text{--}1.478$ . The data are taken at three pointings covering a total area of  $2.33 \text{ arcmin}^2$ , where sensitivity is greater than 50% (Figure 1). Integration time is 1.04 hr per each pointing.

Calibration of the raw data was conducted using the Common Astronomy Software Applications (CASA; McMullin et al. 2007) with a standard pipeline. The calibrated visibilities were inverted using natural weighting to produce mosaicked 3D cubes with different velocity resolutions (50, 100, 200, 400, and  $600 \text{ km s}^{-1}$ ). The synthesized beam size is  $1''.79 \times 1''.41$ , with a position angle of  $-80^\circ$ . Typical noise levels of these cubes are 0.17, 0.12, 0.11, 0.12, and  $0.12 \text{ mJy beam}^{-1}$ . Note that the noise levels are measured by taking the standard deviation of the counts in all the cubes, including pixels with emission, and thus giving upper limits of the noise levels. Then, emission lines are extracted (see the next section for the detailed procedure), and image deconvolution is performed with a CLEAN threshold of  $5\sigma$  for each cube, where we set CLEAN boxes of  $2'' \times 2''$ , almost the same as the synthesized beam size, at the position of each emitter.

The optical and NIR spectroscopies already confirm 34 cluster member galaxies within a radius of  $R_{200}$  (Hilton et al. 2010; Hayashi et al. 2011). We have created catalogs of [O II] emission-line galaxies selected with two narrowband filters, NB912 and NB921 (Hayashi et al. 2014). Among the confirmed member galaxies, 20 galaxies are [O II] emitters. We also retrieve *Hubble Space Telescope* (*HST*) data taken with Wide Field Camera 3 (WFC3; GO-13687, PI: A. Beifiori) from the *HST* archive. All these data are used to search for optical

and NIR counterparts of the emission lines detected in our ALMA Band 3 data.

## 3. CO(2–1) Emission Lines from Cluster Galaxies

We run Clumpfind (Williams et al. 1994) on the data cube without the primary beam correction to search for emission lines, where we adopt the source extraction parameters of  $\Delta T = 2\sigma$  and  $T_{\text{low}} = 5\sigma$ . The emission line search is performed in the cubes with different velocity resolutions of 50, 100, 200, 400, and  $600 \text{ km s}^{-1}$ . We find 8, 7, 5, 7, and 7 emission line candidates at  $>5\sigma$  in each cube, and after excluding overlaps we have detected 21 candidates at a signal-to-noise ratio (S/N) of  $>5.0$  in at least one velocity resolution. Note that we performed the same procedure in the CLEANed cubes, but we find that the number of line candidates detected does not change. This is because the impact of side lobes is almost negligible thanks to the good  $uv$  coverage of the ALMA data taken with 38–42 antennas.

In order to check the reliability of the extracted emission line candidates, we performed the line search in the inverted data cubes in the same manner by counting negative detections. We find 0, 0, 0, 2, and 3 negative detections in the data cubes with 50, 100, 200, 400, and  $600 \text{ km s}^{-1}$  resolution, respectively. This implies that there can be about five false detections at  $>5\sigma$  in our line search.

To remove the possible false detections, we cross-matched the coordinates of the detections in the ALMA data with those of the objects in the optical and NIR data catalogs by Hayashi et al. (2014). We used a search radius of 1 arcsec for the object matching. We found that 17 line candidates have counterparts in the optical–NIR data: 11 have counterparts of [O II] emitters, and 5 have counterparts of sBzK galaxies (Daddi et al. 2004). For the remaining line, #15, the counterpart is not an [O II] emitter, and also it does not have colors that meet the sBzK color criteria. However, #15 seems to be a pair of galaxies with #16, judging from the small spatial separation of  $\sim 0.9 \text{ arcsec}$  and the same central frequency of the lines (Figures 2–3). Four of the detections have no counterparts in the optical and NIR data, which are selected from the data with a  $600 \text{ km s}^{-1}$  resolution only. In this Letter, we remove these emission line candidates without optical/NIR counterparts from the list of emission lines detected. Note that this is consistent with the rate of false detection that we estimate.

A list of the 17 emission lines is given in Table 1, and their spectra are shown in Figure 2. All the detected emission lines have a single Gaussian profile and none have a double peaked profile (Figure 2). We measure the frequency at the peak of an emission line, its width, and the peak line flux by fitting a Gaussian kernel to the spectrum. The width of the lines ranges from 207 to  $593 \text{ km s}^{-1}$ . For 6 of the 17 emission lines, the redshifts measured by the optical and NIR spectroscopies are in good agreement with the redshifts measured from the ALMA data by assuming that they are CO(2–1) lines. Among the emission lines without any spectroscopic redshifts, we can still estimate redshifts for five lines by combining the narrowband imaging data of the adjacent two filters, NB912 and NB921 (Hayashi et al. 2014). Most of the redshifts thus determined are consistent with those of CO(2–1) lines.

Based on the considerations, we regard the 17 lines we have detected with ALMA as CO(2–1) lines from cluster member galaxies. We estimate the CO(2–1) luminosities from the intensity map integrated in velocity by the width of the emission line ( $2 \times \text{FWHM}$ ), following Solomon et al. (1992). The luminosity,  $L'_{\text{CO}(2-1)}$ , ranges  $(4.5\text{--}22) \times 10^9 \text{ K km}^{-1} \text{ pc}^2$ . The properties of the CO(2–1) lines are summarized in Table 1,

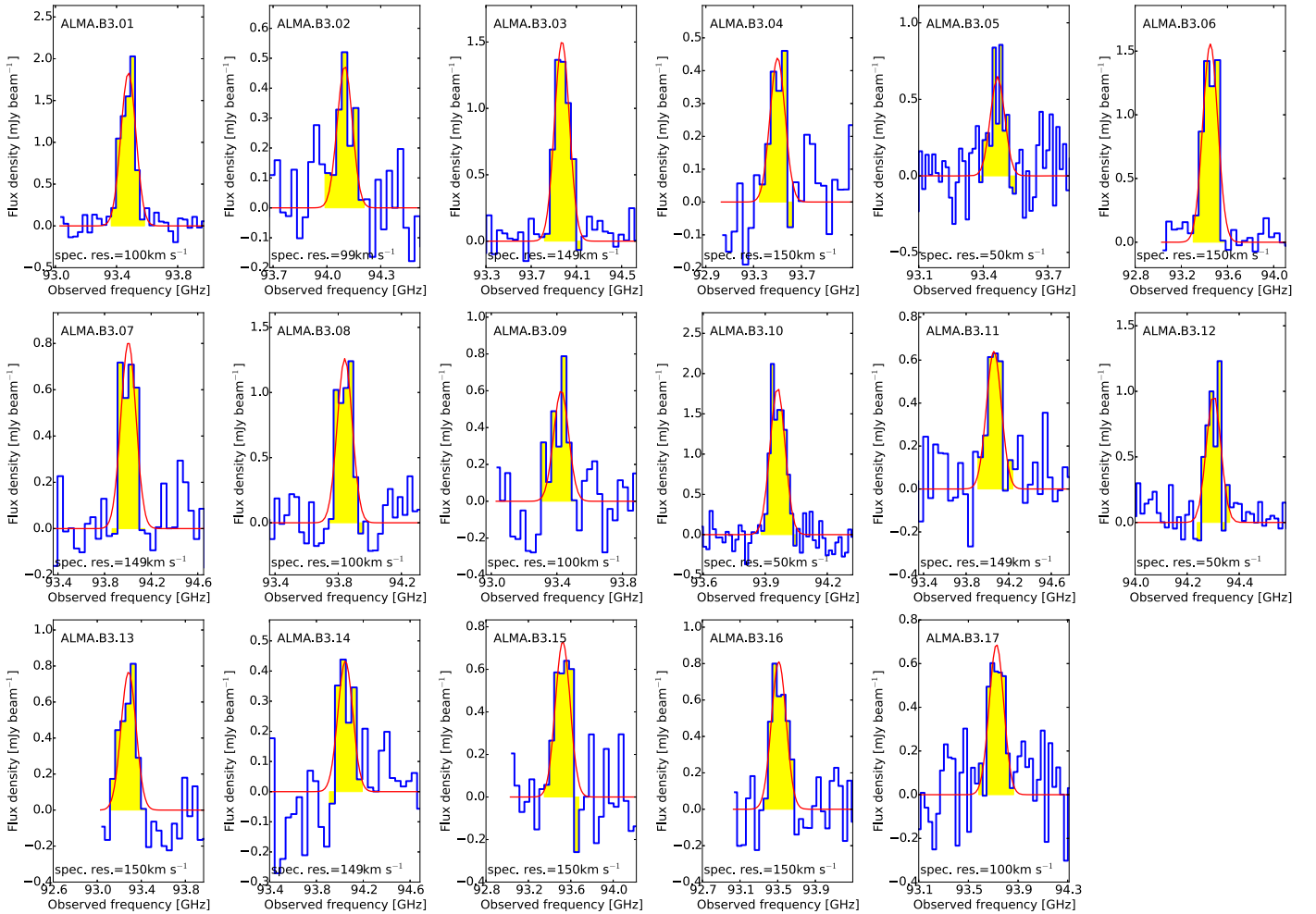


**Figure 2.** Spectra of the CO(2–1) emission lines, where the primary beam attenuation is corrected. The blue line in each panel shows a binned spectrum, where the spectral resolution of the binned spectrum is shown in each panel. The red curve shows the best-fit Gaussian for the emission line highlighted in yellow. The redshift, line width, and luminosity are shown in Table 1.

and their intensity maps are shown in Figure 3. The detection of 17 CO(2–1) emissions in  $2.33 \text{ arcmin}^2$  indicates that the number density of CO(2–1) emitters is several tens of times larger than that expected from the CO luminosity function in the general fields (Walter et al. 2014; Decarli et al. 2016).

The spatial distribution of the CO emitters indicates that there is no detection of a CO emission line in the very center of this cluster, i.e.,  $R < 0.14R_{200}$  or 0.11 Mpc (Figure 1). The trend is clearly seen in the top panel of Figure 4, which shows the cumulative fraction of galaxy populations as a function of distance from the cluster center. The star-forming [O II] emitters tend to be more centrally concentrated than the CO emitters. Member galaxies that are neither [O II] nor CO emitters seem to be located even closer to the cluster center, although their distribution can be affected by a sampling bias in spectroscopic confirmation. This is because [O II] and CO emitters are surveyed in the narrowband imaging or the cubic data all over the field of view, while the other members are confirmed by slit spectroscopy. In addition, the redshifts of the CO emitters show a bimodal distribution with the peaks at  $z \sim 1.452$  and  $1.466$  as if they avoid the central redshift of the cluster at  $z = 1.457$ , as shown in the right panel of Figure 4. On the other hand, the [O II] emitters are distributed around the cluster redshift. The results suggest that there is a difference in the spatial distributions of galaxy populations between gas-rich

galaxies with detections of CO emission lines and those without detections.

## 4. Discussion

### 4.1. Phase-space Diagram

The phase-space diagram is a useful tool to characterize the accretion state of cluster member galaxies relatively free from effects due to the 2D projected positions with respect to the cluster center (Noble et al. 2013, 2016; Muzzin et al. 2014; Jaffé et al. 2015). If the motions of member galaxies are virialized around the cluster center, the line-of-sight velocities have larger dispersions toward the cluster center and lower dispersions at larger radii. Galaxies that are accreted to the cluster recently tend to be offset from that virialized relation and tend to show large relative velocities at any radii. Jaffé et al. (2015) define the “virialized” region, as shown in gray in Figure 4, according to the orbits of dark matter halos in the potential of a galaxy cluster based on a cosmological simulation including a model of ram-pressure. Noble et al. (2013, 2016) divide the phase-space into four areas (central, intermediate, recently accreted, and infalling regions), with curves of constant (velocity)  $\times$  (distance) to separate the accretion states of cluster member galaxies. These defined areas on the phase-space diagram are used to interpret our data.

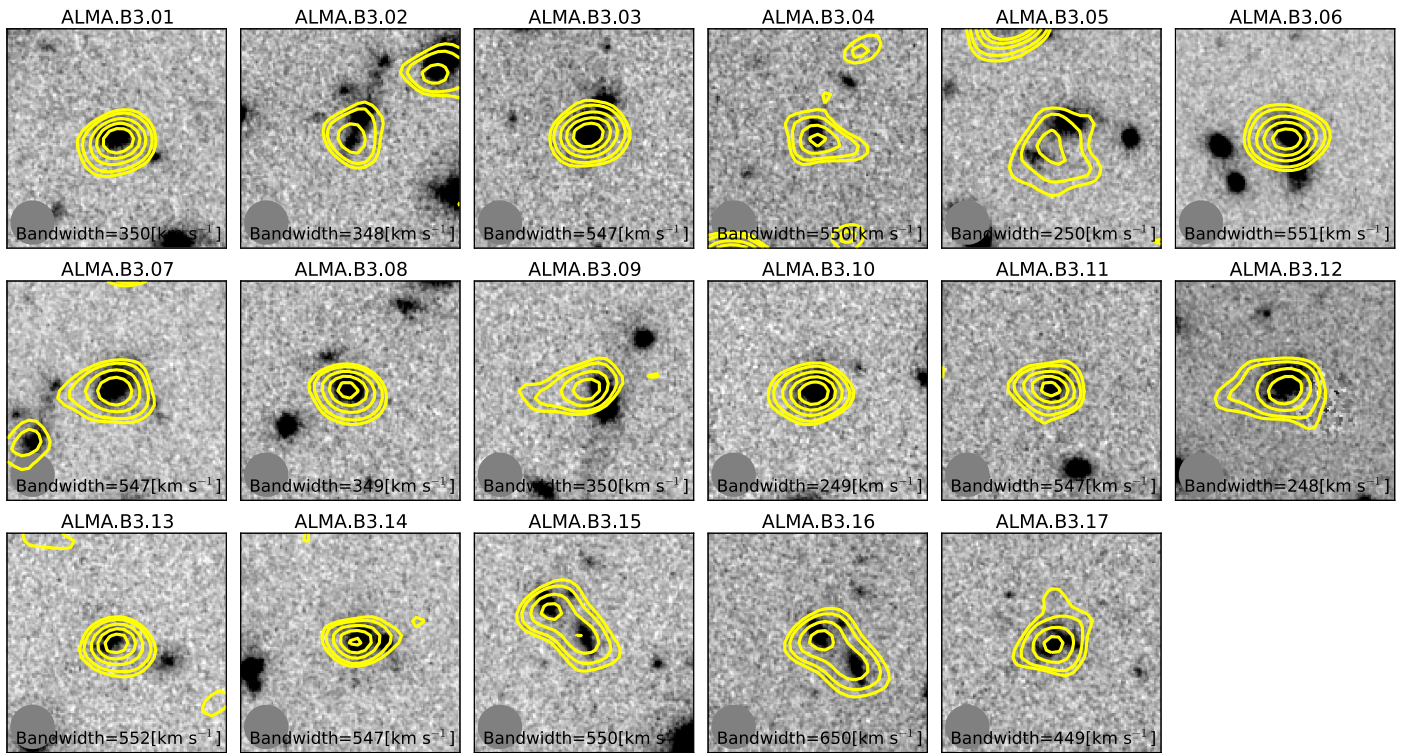


**Figure 3.** Intensity maps of individual CO(2–1) lines overlaid on the *HST*/WFC3 F160W images of 7.5 arcsec each on a side. The contours show the intensity map integrated over a FWHM of each line around the peak frequency at  $1.5\sigma$ ,  $2.0\sigma$ ,  $3.0\sigma$ ,  $4.0\sigma$ , and  $5.0\sigma$  levels. The binned bandwidth is shown in units of  $\text{km s}^{-1}$  at the bottom of each panel. The synthesized beam size (spatial resolution) is shown in gray in the lower left corner.

Figure 4 shows that the CO emitters tend to be distributed at the edge of the virialized region or in the region of relatively recent accretion, while most of the [O II] emitters without CO detections, and the other member galaxies that do not have strong [O II] and CO emissions, tend to be in the virialized region. The five CO emitters (29%) are in the “central” phase-space of  $(\Delta v/\sigma) \times (\Delta R/R_{200}) < 0.2$  defined by Noble et al. (2016), while the 17 [O II] emitters and other member galaxies (55%) are in the same phase-space. Note that among the member galaxies without strong [O II] and CO emissions, some galaxies are red quiescent galaxies and the others have a flux or equivalent width of [O II] emission that is detectable by spectroscopy but is less than the detection limit of our narrowband imaging (Hilton et al. 2010; Hayashi et al. 2014). Therefore, the gas-rich galaxies with CO detections have spent only relatively short times within the cluster. They are likely to begin undergoing the influence of environmental effects acting on galaxies during the course of infall to the cluster. The other member galaxies with amounts of gas smaller than the detection limit tend to have spent longer times as members of the cluster.

#### 4.2. Implications for the Evolution of Cluster Galaxies

Because each quenching mechanism is effectively at work in a specific environment (Treu et al. 2003), the dependence of a gas reservoir on the locations in the phase-space diagram may have strong implications for the physical processes involved in the evolution of the cluster galaxies. Based on the above results, the following scenarios can be considered.

Let us first consider star-forming galaxies in the general fields at  $z \sim 1.5$  or in the outskirts of the cluster. They must have a massive gas reservoir with a gas mass fraction of  $\sim 0.4$

on average, according to previous studies (e.g., Saintonge et al. 2013). When the galaxies are accreted onto the cluster, the first mechanisms that can be at work include galaxy mergers or harassment. Indeed, a merger of gas-rich galaxies (#15 and #16) is observed in the outer region at  $R \sim 0.5R_{200}$ . Then, because this cluster has hot gas exposing the extended X-ray emission (Stanford et al. 2006), during the passage of a cluster core galaxies would suffer from ram-pressure stripping and the gas trapped in the galaxies would be removed from the systems. The main component of the stripped gas is H I gas (e.g., Kenney et al. 2004) and the molecular gas is relatively much less affected by the ram-pressure (e.g., Lee et al. 2017). This is supported by the fact that the intensity maps of all CO lines but #09 are in good agreement with the stellar component of the galaxies (Figure 3). Therefore, CO(2–1) emission lines can be detected in the galaxies in the accretion region of the phase-space diagram (Figure 4). The CO(2–1) luminosities correspond to  $M_{\text{H}_2} = (2.0\text{--}9.4) \times 10^{10} M_{\odot}$ , under the assumptions of  $L'_{\text{CO}(2-1)}/L'_{\text{CO}(1-0)} = 1$  (Dannerbauer et al. 2009), and  $\alpha_{\text{CO}} = 4.36$  (Tacconi et al. 2013). Since the star-forming member galaxies have the SFRs of several dozens of  $M_{\odot} \text{ yr}^{-1}$  (the median SFR =  $88 M_{\odot} \text{ yr}^{-1}$ ) (Hayashi et al. 2010), the depletion timescale is estimated to be of the order of  $\sim 10^9$  years. This is comparable to the typical dynamical timescale of galaxy clusters (Frenk et al. 1996). The order estimation suggests that it is possible that a gas reservoir of a galaxy is fully consumed by newly formed stars before it settles into the virialized region, unless new fuel is supplied to the galaxy. If a starvation mechanism is at work in a cluster galaxy, the H I gas is stripped from the reservoir and the galaxy’s supply of fresh gas is terminated. The molecular gas is consumed rapidly by the remaining star formation, and star formation activity is eventually truncated.

**Table 1**  
Properties of CO(2–1) Emission Lines

ID	R.A. (J2000)	Decl. (J2000)	Redshift <sup>a</sup>	Line Width (10 <sup>2</sup> km s <sup>-1</sup> )	$L'_{\text{CO}(2-1)}$ (10 <sup>9</sup> K km s <sup>-1</sup> pc <sup>2</sup> )	S/N	Counterpart
ALMA.B3.01	22 15 58.16	-17 38 14.5	1.466	3.7 ± 0.2	19.9 ± 1.1	18.8	NB921 [O II]
ALMA.B3.02	22 15 57.51	-17 38 00.5	1.450	3.1 ± 0.8	4.5 ± 0.9	4.7	sBzK
ALMA.B3.03	22 15 58.54	-17 37 47.7	1.453	4.9 ± 0.3	21.6 ± 1.2	18.6	NB921 [O II]
ALMA.B3.04	22 15 59.52	-17 37 54.2	1.466	4.8 ± 1.1	6.2 ± 1.2	5.3	sBzK
ALMA.B3.05	22 15 58.05	-17 38 18.7	1.467	2.5 ± 0.6	4.7 ± 0.9	5.1	NB921 [O II]
ALMA.B3.06	22 15 59.72	-17 37 59.0	1.467	4.9 ± 0.4	21.2 ± 1.2	18.0	NB921 [O II]
ALMA.B3.07	22 15 57.28	-17 37 58.0	1.452	4.8 ± 0.7	11.0 ± 1.2	9.5	sBzK
ALMA.B3.08	22 15 58.23	-17 38 22.2	1.457	3.6 ± 0.4	12.2 ± 1.0	11.7	sBzK
ALMA.B3.09	22 15 57.76	-17 37 45.2	1.468	3.5 ± 0.7	6.8 ± 1.0	6.8	NB912+NB921 [O II]
ALMA.B3.10	22 15 57.23	-17 37 53.2	1.454	2.7 ± 0.2	14.0 ± 0.9	15.4	NB912+NB921 [O II]
ALMA.B3.11	22 15 58.75	-17 37 41.0	1.451	5.3 ± 1.0	9.6 ± 1.2	8.0	NB912+NB921 [O II]
ALMA.B3.12	22 15 56.92	-17 38 05.0	1.445	2.1 ± 0.3	5.6 ± 0.8	7.3	NB912 [O II]
ALMA.B3.13	22 15 59.77	-17 38 16.7	1.471	5.2 ± 0.7	10.6 ± 1.2	8.5	sBzK
ALMA.B3.14	22 16 00.41	-17 37 50.7	1.451	4.8 ± 1.0	6.2 ± 1.1	5.4	NB912 [O II]
ALMA.B3.15	22 16 00.83	-17 38 32.5	1.465	5.2 ± 0.9	10.9 ± 1.2	8.9	
ALMA.B3.16	22 16 00.92	-17 38 31.5	1.465	5.9 ± 0.8	13.6 ± 1.3	10.6	NB921 [O II]
ALMA.B3.17	22 16 00.38	-17 38 57.7	1.460	4.4 ± 0.8	8.9 ± 1.1	8.2	NB912+NB921 [O II]

**Note**

<sup>a</sup> The redshifts are derived from CO(2–1) emission lines.

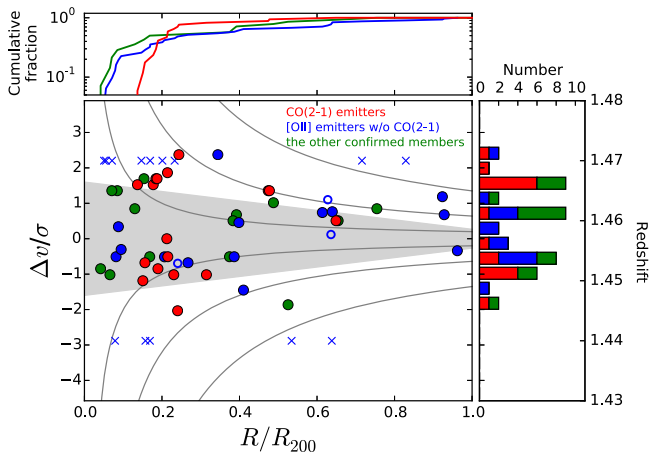


**Figure 4.** Phase-space diagram showing the relative line-of-sight velocities of cluster member galaxies as a function of distance from the cluster center. The red circles show the CO(2–1) emitters. The blue symbols show the [O II] emitters without CO(2–1) detection, among which the filled circles represent the spectroscopically confirmed ones, while the open circles are those with redshifts estimated from the ratio of emission line fluxes of two adjacent narrowband filters (NB912 and NB921), and the crosses are those detected only either in NB912 or NB921 (Hayashi et al. 2014). We set those redshifts to be 1.44 (for NB912) and 1.47 (for NB921), respectively. Green circles show the other spectroscopically confirmed cluster members (Hilton et al. 2010; Hayashi et al. 2014). The gray region shows a virialized area defined by Jaffé et al. (2015). The gray lines show the curves of constant  $v \times R$  values (Noble et al. 2016). (right panel) Redshift histograms of spectroscopically confirmed galaxies. (upper panel) Cumulative fraction of the number of galaxies as a function of radius from the cluster center.

Since no CO emission line is detected at the very center of the cluster, starvation, as well as ram-pressure stripping, are likely at work in the galaxies. By the time the galaxies settle in the virialized region of the central region, the star formation activity is fully quenched.

To verify our scenario, information on HI gas is also important, in addition to knowledge of the molecular gas. It is still impossible to observe HI gas in and around galaxies at  $z > 1$ , however, there were several observations of HI gas in cluster galaxies at lower

redshifts of  $z \lesssim 0.2$  (e.g., Verheijen et al. 2007; Lah et al. 2009; Jaffé et al. 2015; Stroe et al. 2015). Jaffé et al. (2015) present the result of HI gas survey in a massive galaxy cluster at  $z = 0.2$  and find that almost all of the HI detected galaxies are located in the recent infall region in the phase-space. They argue that the ram-pressure plays a key role in removing the HI gas from the galaxies. This supports our scenario.

Investigating the detailed properties of individual galaxies and their dependence in the positions on the phase-space diagram can deepen our insight into the evolution of cluster galaxies. So far, there is no (proto-)cluster at  $z > 1$  that has a detection of CO emissions that is statistically sufficient to discuss the molecular gas properties of the member galaxies on the phase-space diagram. This study, for the first time, succeeds in detecting CO(2–1) emission lines from the 17 member galaxies in the cluster at  $z = 1.46$ . For a better understanding of the evolution of cluster galaxies, identification of the mode of star formation, i.e., as a starburst or secular, and the efficiency of star formation, are key factors (Daddi et al. 2010; Genzel et al. 2010). We will discuss these issues in forthcoming papers.

We thank the anonymous referee for providing constructive comments and suggestions. M.H. acknowledges the financial support by JSPS Grant-in-Aid for Young Scientists (A) Grant Number JP26707006. T.K. acknowledges the financial support in part by a Grant-in-Aid for Scientific Research (Nos. 21340045 and 24244015) by the Japanese Ministry of Education, Culture, Sports and Science. Y.T. was supported by JSPS Grant-in-Aid for Scientific Research (A) Number 15H02073. K.K. was supported by JSPS Grant-in-Aid for Scientific Research (A) Number 25247019. This paper makes use of the following ALMA data: ADS/JAO.ALMA#2015.1.00779.S. ALMA is a partnership of ESO, NSF (USA) and NINS (Japan), together with NRC (Canada), NSC and ASIAA (Taiwan), and KASI (Republic of Korea), in cooperation with the Republic of Chile. The Joint ALMA Observatory is operated by ESO, AUI/NRAO, and NAOJ.

Facility: ALMA.

## References

- Aravena, M., Carilli, C. L., Salvato, M., et al. 2012, *MNRAS*, **426**, 258
- Carilli, C. L., & Walter, F. 2013, *ARA&A*, **51**, 105
- Casasola, V., Magrini, L., Combes, F., et al. 2013, *A&A*, **558**, A60
- Daddi, E., Cimatti, A., Renzini, A., et al. 2004, *ApJ*, **617**, 746
- Daddi, E., Elbaz, D., Walter, F., et al. 2010, *ApJL*, **714**, L118
- Dannerbauer, H., Daddi, E., Riechers, D. A., et al. 2009, *ApJL*, **698**, L178
- Dannerbauer, H., Lehnert, M. D., Emonts, B. H. C., et al. 2017, *A&A*, submitted (arXiv:1701.05250)
- Decarli, R., Walter, F., Aravena, M., et al. 2016, *ApJ*, **833**, 69
- Dressler, A., Oemler, A., Jr., Couch, W. J., et al. 1997, *ApJ*, **490**, 577
- Frenk, C. S., Evrard, A. E., White, S. D. M., & Summers, F. J. 1996, *ApJ*, **472**, 460
- Geach, J. E., Smail, I., Moran, S. M., et al. 2011, *ApJL*, **730**, L19
- Genzel, R., Tacconi, L. J., Gracia-Carpio, J., et al. 2010, *MNRAS*, **407**, 2091
- Genzel, R., Tacconi, L. J., Lutz, D., et al. 2015, *ApJ*, **800**, 20
- Hayashi, M., Kodama, T., Koyama, Y., et al. 2010, *MNRAS*, **402**, 1980
- Hayashi, M., Kodama, T., Koyama, Y., et al. 2014, *MNRAS*, **439**, 2571
- Hayashi, M., Kodama, T., Koyama, Y., Tadaki, K.-I., & Tanaka, I. 2011, *MNRAS*, **415**, 2670
- Hilton, M., Lloyd-Davies, E., Stanford, S. A., et al. 2010, *ApJ*, **718**, 133
- Ivison, R. J., Swinbank, A. M., Smail, I., et al. 2013, *ApJ*, **772**, 137
- Jaffé, Y. L., Smith, R., Candlish, G. N., et al. 2015, *MNRAS*, **448**, 1715
- Kenny, J. D. P., van Gorkom, J. H., & Vollmer, B. 2004, *AJ*, **127**, 3361
- Lah, P., Pracy, M. B., Chengalur, J. N., et al. 2009, *MNRAS*, **399**, 1447
- Lee, B., Chung, A., Tonnesen, S., et al. 2017, *MNRAS*, **466**, 1382
- Lilly, S. J., Carollo, C. M., Pipino, A., Renzini, A., & Peng, Y. 2013, *ApJ*, **772**, 119
- Ma, C.-J., Smail, I., Swinbank, A. M., et al. 2015, *ApJ*, **806**, 257
- McMullin, J. P., Waters, B., Schiebel, D., Young, W., & Golap, K. 2007, in ASP Conf. Ser. 376, *Astronomical Data Analysis Software and Systems XVI*, ed. R. A. Shaw, F. Hill, & D. J. Bell (San Francisco, CA: ASP), 127
- Muzzin, A., van der Burg, R. F. J., McGee, S. L., et al. 2014, *ApJ*, **796**, 65
- Noble, A. G., Webb, T. M. A., Muzzin, A., et al. 2013, *ApJ*, **768**, 118
- Noble, A. G., Webb, T. M. A., Yee, H. K. C., et al. 2016, *ApJ*, **816**, 48
- Peng, Y.-j., Lilly, S. J., Kovač, K., et al. 2010, *ApJ*, **721**, 193
- Saintonge, A., Lutz, D., Genzel, R., et al. 2013, *ApJ*, **778**, 2
- Scoville, N., Arnouts, S., Aussel, H., et al. 2013, *ApJS*, **206**, 3
- Seko, A., Ohta, K., Yabe, K., et al. 2016, *ApJ*, **819**, 82
- Silverman, J. D., Daddi, E., Rodighiero, G., et al. 2015, *ApJL*, **812**, L23
- Solomon, P. M., Downes, D., & Radford, S. J. E. 1992, *ApJL*, **398**, L29
- Stanford, S. A., Romer, A. K., Sabirli, K., et al. 2006, *ApJL*, **646**, L13
- Stroe, A., Oosterloo, T., Röttgering, H. J. A., et al. 2015, *MNRAS*, **452**, 2731
- Tacconi, L. J., Genzel, R., Neri, R., et al. 2010, *Natur*, **463**, 781
- Tacconi, L. J., Genzel, R., Saintonge, A., et al. 2017, *ApJ*, submitted (arXiv:1702.01140)
- Tacconi, L. J., Neri, R., Genzel, R., et al. 2013, *ApJ*, **768**, 74
- Tadaki, K.-i., Kodama, T., Tamura, Y., et al. 2014, *ApJL*, **788**, L23
- Treu, T., Ellis, R. S., Kneib, J.-P., et al. 2003, *ApJ*, **591**, 53
- Verheijen, M., van Gorkom, J. H., Szomoru, A., et al. 2007, *ApJL*, **668**, L9
- Walter, F., Decarli, R., Sargent, M., et al. 2014, *ApJ*, **782**, 79
- Williams, J. P., de Geus, E. J., & Blitz, L. 1994, *ApJ*, **428**, 693
- Zahid, H. J., Dima, G. I., Kudritzki, R.-P., et al. 2014, *ApJ*, **791**, 130